

A TENSOR DECOMPOSITION APPROACH FOR HIGH-DIMENSIONAL HAMILTON-JACOBI-BELLMAN EQUATIONS

SERGEY DOLGOV*, DANTE KALISE†, AND KARL KUNISCH‡

Abstract. A tensor decomposition approach for the solution of high-dimensional, fully nonlinear Hamilton-Jacobi-Bellman equations arising in optimal feedback control and estimation of nonlinear dynamics is presented. The proposed method combines a tensor train approximation for the value function together with a Newton-like iterative method for the solution of the resulting nonlinear system. The effectiveness of tensor approximations circumvents the curse of dimensionality, solving Hamilton-Jacobi equations with more than 100 dimensions at modest cost. The linear scaling of the computational complexity with respect to the dimension allows to solve PDE-constrained optimal feedback control problems over high-dimensional state spaces. Numerical tests including the control of a 2D nonlinear reaction equation and the stabilization of a bilinear Fokker-Planck equation are presented.

Key words. Optimal Feedback Control, Hamilton-Jacobi-Bellman Equations, Nonlinear Dynamics, Tensor Calculus, High-dimensional Approximation, Tensor Train Decomposition

AMS subject classifications. 49J20, 49LXX, 49MXX, 15A69, 15A23, 65F10, 65N22, 65D15

1. Introduction. Richard Bellman first coined the expression “curse of dimensionality” when referring to the overwhelming computational complexity associated to the solution of multi-stage decision processes through dynamic programming, what is nowadays known as Bellman’s equation. More than 60 years down the road, the curse of dimensionality has become ubiquitous in different fields such as numerical analysis, compressed sensing and statistical machine learning. However, it is in the computation of optimal feedback policies for the control of dynamical systems where its meaning continues to be most evident. Here, the curse of dimensionality arises since the synthesis of optimal feedback laws by dynamic programming techniques demands the solution of a Hamilton-Jacobi-Bellman (HJB) fully nonlinear Partial Differential Equation (PDE) cast over the state space of the dynamics. This intrinsic relation between the dimensions of the state space of the control system and the domain of the HJB PDE generates computational challenges of formidable complexity even for relatively simple dynamical systems¹. Much of the research in control revolves around circumventing this barrier through different trade-offs between dimensionality, performance, and optimality of the control design. Prominent examples of the research landscape shaped by the curse of dimensionality include model order reduction, model predictive control, suboptimal feedback design, reinforcement learning and distributed control, to name just a few. However, the effective computational solution of dynamic programming equations of arbitrarily high dimensions through deterministic methods

*S. Dolgov is with the Department of Mathematical Sciences, University of Bath, North Rd, BA2 7AY Bath, United Kingdom (S.Dolgov@bath.ac.uk). S. Dolgov is thankful to Engineering and Physical Sciences Research Council for the support through Fellowship EP/M019004/1.

†D. Kalise is with the Department of Mathematics, Imperial College London, South Kensington Campus, SW7 2AZ London, United Kingdom (dkaliseb@ic.ac.uk).

‡K. Kunisch is with Institute of Mathematics and Scientific Computing, University of Graz, Heinrichstr. 36, A-8010 Graz, Austria and Radon Institute for Computational and Applied Mathematics (RICAM), Altenbergerstraße 69, A-4040 Linz, Austria (karl.kunisch@uni-graz.at).

¹As an illustration, consider the simplest double integrator dynamics $\dot{x} = u$, whose optimal feedback synthesis already requires the solution of a two-dimensional PDE. For a quadcopter model where the dynamics are described by a 12-dimensional nonlinear dynamical system, the associated HJB PDE has to be solved in \mathbb{R}^{12} . Bear in mind that much of the research in computational PDEs is devoted to the solution of problems in physical space, that is \mathbb{R}^{3+1} , at most.

remains an open quest with fundamental implications in optimal control design. Our contribution in the present work is to develop a computational approach based on tensor calculus techniques for the solution of high-dimensional HJB PDEs arising in optimal feedback control of systems governed by partial differential equations. We show that for a wide class of evolution equations, our technique scales linearly with the dimension, allowing an accurate control design at a moderate computational cost for dynamics with over 100 dimensions.

1.1. Numerical approximation of HJB PDEs: old and new. The numerical approximation of Hamilton-Jacobi-Bellman equations through computational PDE methods is a well-established topic dating back to the seminal work by Crandall and Lions [13], which has been addressed through a range of discretization strategies, most notably finite differences, level-set methods and semi-Lagrangian schemes (we refer to [16] for an up-to-date survey on discretization methods for HJB). The aforementioned techniques have proven to overcome the difficulties associated to the fully nonlinear character of the HJB PDEs [31]. However, they are inherently grid-based discretization schemes and therefore suffer from the curse of dimensionality. That is, for a multidimensional ansatz defined upon a tensor product of 1d objects, the scaling of the total number of degrees of freedom of the discretized problem grows exponentially with respect to the dimension of the HJB PDE. This makes the problem computationally intractable for dimensions larger than 4. We reiterate this is a fundamental limitation in the context of nonlinear optimal feedback control, where the dimension of the associated HJB PDE is determined by the dimension of the state space of the control system. A partial remedy to this difficulty is the coupling of grid-based discretizations for low-dimensional HJB PDEs with model reduction techniques to lower the dimension of the control system [27, 3]. This approach has proven to be successful for dynamics with strong dissipative properties, however, its overall performance relies on a good state space sampling and deteriorates for dynamics including transport, delays, or highly nonlinear phenomena [20].

Despite the rigorous design of numerical methods for the solution of very high-dimensional HJB PDEs remains largely an open problem, encouraging results have been obtained over the last years. A non-exhaustive list include the use of machine learning techniques [37, 15, 19], approximate dynamic programming in the context of reinforcement learning [8, 34], causality-free methods and convex optimization [23, 12], max-plus algebra methods [29, 5], polynomial approximation [21, 22], tree structure algorithms [4], and sparse grids [10, 17]. A very recent stream of works (including [15, 37, 19, 33] among many others) has explored the application of machine learning techniques to approximate high-dimensional nonlinear PDEs. The work [37] proposes the so-called Deep Galerkin Method, combining the use of a deep neural network ansatz for the solution together with a PDE residual minimization. In [15, 19], the authors focus on the class of time-dependent HJB equations arising in stochastic control where a pointwise evaluation of the solution can be realized through a representation formula involving the solution of a backward stochastic differential equation. These latter approaches can be linked to causality-free methods, with deterministic counterparts explored in [23, 30, 12, 39].

1.2. A tensor calculus framework for nonlinear HJB. In this work we propose a numerical method for the solution of HJB equations based on tensor decomposition techniques [7, 26, 25], which have proven to be successful in tackling the curse of dimensionality in the context of numerical analysis of PDEs [24]. The use of low-rank structures such as the tensor-train (TT) format [32] to represent high-dimensional

objects allows the solution of linear high-dimensional problems by generalizing standard numerical linear algebra techniques to multi-index arrays of coefficients (tensors) and the multivariate functions they approximate. This approach has been recently explored in [18] for solving a class of finite-horizon stochastic control problems where the associated time-dependent HJB PDE can be transformed into a linear equation [38]. Here, we extend the tensor calculus framework to approximate the solution of fully nonlinear, first-order, stationary HJB PDEs arising from deterministic infinite horizon control. Furthermore, through the selection of suitable control penalties [28], our method allows the inclusion of control constraints in the design.

1.3. Towards optimal feedback control of PDEs. While high-dimensional control systems naturally arise in aerospace engineering [9] and agent-based models [1], the motivation behind our work is the design of optimal feedback laws for systems governed by partial differential equations. From a dynamical perspective, PDEs correspond to abstract, infinite-dimensional systems and therefore the HJB synthesis has to be understood over an infinite-dimensional state space. The theory behind this abstract formulation dates back to the work by Crandall and Lions [14]. From a computational perspective, the treatment is based on the so-called method of lines [35]. Given an evolutionary PDE, we discretize the space dependence either by finite differences/elements or spectral methods, leading to a large-scale dynamical system with as many states as the space discretization dictates. We perform the HJB synthesis over this finite but high-dimensional system. The accuracy of such a representation and its implications over the control design vary depending on the class of PDEs under consideration. For example, strongly dissipative PDEs can be accurately represented with few degrees of freedom in space, while convection-dominated PDEs might require a much more complex state space representation. Therefore, the performance study of our framework with respect to the dimension parameter is central to our analysis. It benefits from the fact that, unlike the nonlinear ODE world, the taxonomy of physically meaningful nonlinearities in time-dependent PDEs is well-delimited. We reduce our analysis to nonlinear reaction PDEs where we take the Newell-Whitehead equation as a reference model due to its rich equilibrium structure, and to nonlinear convection in the Fokker-Planck equation, where the control action enters as a bilinear term. The semi-discretization in space of these nonlinearities leads to well-structured finite-dimensional realizations [21] permitting a more systematic analysis of the scaling of our methodology with respect to the dimension.

2. Methodology. We begin by introducing a precise problem statement concerning optimal feedback synthesis through the Hamilton-Jacobi-Bellman equation. Then, we present the different building blocks constituting the proposed numerical method.

2.1. The Hamilton-Jacobi-Bellman equation in nonlinear control. For the sake of simplicity, we develop our presentation around the following infinite horizon optimal control problem

$$(2.1) \quad \min_{u(\cdot) \in \mathcal{U}} \mathcal{J}(u(\cdot), \mathbf{x}) := \int_0^{\infty} \ell(\mathbf{y}(t)) + \gamma |u(t)|^2 dt,$$

subject to the nonlinear dynamical constraint

$$(2.2) \quad \dot{\mathbf{y}}(t) = \mathbf{f}(\mathbf{y}(t)) + \mathbf{g}(\mathbf{y})u(t), \quad \mathbf{y}(0) = \mathbf{x},$$

where we denote the state $\mathbf{y}(t) = (y_1(t), \dots, y_d(t))^\top \in \mathbb{R}^d$, the control $u(\cdot) \in \mathcal{U}$, with $\mathcal{U} = \{u(t) : \mathbb{R}_+ \rightarrow U \subset \mathbb{R}\}$, the state running cost $\ell(\mathbf{y}) : \mathbb{R}^d \rightarrow \mathbb{R}^+$, and the control penalization $\gamma > 0$. We assume the running cost $\ell(\mathbf{y})$ and the system dynamics $\mathbf{f}(\mathbf{y}) : \mathbb{R}^d \rightarrow \mathbb{R}^d$ and $\mathbf{g}(\mathbf{y}) : \mathbb{R}^d \rightarrow \mathbb{R}^d$ to be $\mathcal{C}^1(\mathbb{R}^d)$. Without loss of generality, the origin $\mathbf{y} = \mathbf{0}$ is an equilibrium of the uncontrolled dynamics and $\mathbf{g}(\mathbf{0}) = \ell(\mathbf{0}) = 0$. Under these definitions, the control problem (2.1)-(2.2) corresponds to the design of a globally asymptotically stabilizing control signal $u(t)$. A natural synthesis method for this problem is the use of dynamic programming techniques. By defining the value function

$$(2.3) \quad V(\mathbf{x}) := \inf_{u(\cdot) \in \mathcal{U}} J(u(\cdot), \mathbf{x})$$

we characterize the solution of the infinite horizon control problem as the unique viscosity solution of the Hamilton-Jacobi-Bellman equation

$$(2.4) \quad \min_{u \in U} \{(\mathbf{f}(\mathbf{x}) + \mathbf{g}(\mathbf{x})u)^\top DV(\mathbf{x}) + \ell(\mathbf{x}) + \gamma|u|^2\} = 0, \quad V(0) = 0,$$

where $DV(\mathbf{x}) = (\partial_{x_1} V, \dots, \partial_{x_d} V)^\top$. In the unconstrained case, i.e., $U \equiv \mathbb{R}$, the minimizer u^* in (2.4) can be readily expressed in feedback form as

$$(2.5) \quad u^*(\mathbf{x}) = \arg \min_{u \in \mathbb{R}} \{(\mathbf{f}(\mathbf{x}) + \mathbf{g}(\mathbf{x})u)^\top DV(\mathbf{x}) + \ell(\mathbf{x}) + \gamma|u|^2\} = -\frac{1}{2\gamma} \mathbf{g}(\mathbf{x})^\top DV(\mathbf{x}),$$

which after inserting in (2.4), leads to

$$(2.6) \quad DV(\mathbf{x})^\top \mathbf{f}(\mathbf{x}) - \frac{1}{4\gamma} DV(\mathbf{x})^\top \mathbf{g}(\mathbf{x}) \mathbf{g}(\mathbf{x})^\top DV(\mathbf{x}) + \ell(\mathbf{x}) = 0.$$

The derivation above can be extended to allow controls in \mathbb{R}^m with $m > 1$. It can also be modified to introduce box constraints in the control action through a penalty approach. Following [28], we replace the control penalty $\gamma|u|^2$ by

$$(2.7) \quad W(u) = 2\gamma \int_0^u \mathcal{P}^{-1}(\mu) d\mu,$$

where $\mathcal{P} : \mathbb{R} \rightarrow \mathbb{R}$ is a bounded, integrable, bijective \mathcal{C}^1 function with $W(0) = 0$. The computation of the optimality condition (2.5) leads to

$$(2.8) \quad u^*(\mathbf{x}) = \arg \min_{u \in \mathbb{R}} \{(\mathbf{g}(\mathbf{x})u)^\top DV(\mathbf{x}) + W(u)\} = -\mathcal{P} \left(\frac{1}{2\gamma} \mathbf{g}(\mathbf{x})^\top DV(\mathbf{x}) \right),$$

where we can impose lower and upper bound constraints by choosing penalties of the type $\mathcal{P}(x) = \tanh(x)$.

As already discussed in Section 1, the main computational difficulties in the solution of HJB-type equations are related to the construction of numerical schemes able to effectively handle high-dimensional spaces ($d > 10$), and to the treatment of the nonlinearity. In the following, we discuss these two aspects separately.

2.2. An iterative approach for the solution of HJB equations. The construction of a numerical scheme for (2.4) begins with the application of the so-called Successive Approximation Algorithm [6], which corresponds to a continuous variant

of the well-known policy iteration algorithm in dynamic programming [2, 11]. Conceptually speaking, given an initial guess $u^0(\mathbf{x})$ for the optimal feedback control, we insert it into (2.4) which then becomes a linear PDE for $V(\mathbf{x})$ whose solution dictates the update of the feedback control via (2.5). This procedure turns to be equivalent to the application of a Newton-type method for $V(\mathbf{x})$ directly over (2.6). As it is often the case in the application of Newton-type iterative methods, the convergence of the algorithm is sensitive to its initialization, and therefore we introduce the concept of admissible feedback maps.

DEFINITION 2.1 (Admissible feedback). *We say that a feedback mapping $u := u(\mathbf{x})$ is admissible on $\Omega \subset \mathbb{R}^d$, denoted as $u \in \mathcal{A}(\Omega)$, if $u(\mathbf{x}) \in \mathcal{C}(\Omega)$, $u(\mathbf{0}) = 0$, and $\mathcal{J}(u(\mathbf{y}(\cdot)), \mathbf{x}) < \infty$ for all $\mathbf{x} \in \Omega$.*

Given an admissible feedback $u_0(\mathbf{x})$, the Continuous Policy Iteration Algorithm (Algorithm 2.1) generates a decreasing sequence of values V_s converging to a pair (V^*, u^*) which solves eqn. (2.4) in Ω . The Continuous Policy Iteration Algorithm slightly dif-

Algorithm 2.1 Continuous Policy Iteration Algorithm

- 1: Input: $u_0(\mathbf{x}) \in \mathcal{A}(\Omega)$ and $tol > 0$
 - 2: **while** $error > tol$ **do**
 - 3: Solve the linearized HJB: $(\mathbf{f}(x) + \mathbf{g}(\mathbf{x})u_s)^T DV_s(\mathbf{x}) + \ell(\mathbf{x}) + \gamma|u_s|^2 = 0$.
 - 4: Update the feedback map: $u_{s+1}(\mathbf{x}) = -\frac{1}{2\gamma}\mathbf{g}^\top DV_s(\mathbf{x})$.
 - 5: $error = \|V_s - V_{s-1}\|$, set $s := s + 1$.
 - 6: **end while**
 - 7: **return** $(V_s, u_s) \approx (V^*, u^*)$
-

fers from the standard policy iteration formulation in its requirement of an admissible feedback map, which is often omitted due to the existence of a discount factor.

2.3. The numerical approximation of the HJB equation via tensors.

Each step of the Successive Approximation Algorithm requires the solution of the linear, but high-dimensional PDE

$$(2.9) \quad (\mathbf{f}(\mathbf{x}) + \mathbf{g}(\mathbf{x})u_s(\mathbf{x}))^\top DV_s(\mathbf{x}) + \ell(\mathbf{x}) + \gamma|u_s(\mathbf{x})|^2 = 0, \quad s = 0, 1, \dots$$

Standard finite/spectral element discretization in each coordinate would result in the *curse of dimensionality*, i.e. the number of degrees of freedom growing exponentially in d . In this section we introduce the low-rank tensor decompositions that allow to approximate the discrete coefficients of V_s with much fewer unknowns. First, we outline the particular discretization scheme used throughout the paper. For brevity, we omit the iteration index s in (2.9) and denote V_s simply by V , and u_s by \tilde{u} .

2.3.1. Discretizing the HJB equation. We follow [21] closely and employ the Galerkin spectral element approximation. The main difference is the construction of the basis functions from the polynomials of bounded maximal *individual* degree, in contrast to the maximal *total* degree ansatz in [21]. Subsequently the curse of dimensionality of the maximal individual degree scheme will be circumvented on the discrete level.

Concretely, we introduce a space of tensorised Legendre polynomials of maximal individual degree $n - 1$,

$$(2.10) \quad \mathcal{V}_n = \text{span} \{ \Phi_{\mathbf{i}}(\mathbf{x}) := \phi_{i_1}(x_1) \cdots \phi_{i_d}(x_d), \quad i_k = 0, \dots, n - 1, \quad k = 1, \dots, d \},$$

where $\phi_{i_k}(x_k)$ are the univariate Legendre polynomials of degree $i_k \leq n-1$, and the multi-index $\mathbf{i} = (i_1, \dots, i_d)$. The value function approximation is sought in \mathcal{V}_n by making the Galerkin residual vanish on \mathcal{V}_n . We make the ansatz

$$(2.11) \quad V(x_1, \dots, x_d) \approx \sum_{j_1, \dots, j_d=0}^{n-1} \mathbf{v}(j_1, \dots, j_d) \Phi_{j_1, \dots, j_d}(\mathbf{x}),$$

and solve a system of n^d Galerkin equations in n^d unknowns of \mathbf{v} ,

$$(2.12) \quad \sum_{\mathbf{j}} \langle \Phi_{\mathbf{i}}, (\mathbf{f} + \mathbf{g}\ddot{u})^\top D\Phi_{\mathbf{j}} \rangle_{L^2(\Omega)} \mathbf{v}(\mathbf{j}) = - \langle \Phi_{\mathbf{i}}, \ell + \gamma \ddot{u}^2 \rangle_{L^2(\Omega)},$$

where $\Omega = (-a, a)^d$ with an appropriately chosen *domain size* a .

REMARK 1. *Due to the tensor product subspace (2.10), the approximation accuracy of (2.11) can be analyzed using standard univariate polynomial approximation theory [61]. For example, if $V(\mathbf{x}) \in C^p(\Omega)$, the discretization error decays with an $\mathcal{O}(n^{-p})$ rate.*

2.3.2. The TT format. The coefficients in (2.11) are enumerated by d independent indices, so \mathbf{v} can be treated as a d -dimensional *tensor*. Throughout the paper, we approximate such tensors by the so-called Tensor Train (TT) decomposition [32],

$$(2.13) \quad \mathbf{v}(i_1, \dots, i_d) \approx \tilde{\mathbf{v}}(i_1, \dots, i_d) := \sum_{\alpha_0, \dots, \alpha_d=1}^{r_0, \dots, r_d} \mathbf{v}_{\alpha_0, \alpha_1}^{(1)}(i_1) \mathbf{v}_{\alpha_1, \alpha_2}^{(2)}(i_2) \cdots \mathbf{v}_{\alpha_{d-1}, \alpha_d}^{(d)}(i_d).$$

The smaller (3-dimensional) tensors $\mathbf{v}^{(k)}$ on the right hand side are called *TT blocks*, and the new summation ranges r_0, \dots, r_d are called *TT ranks*. Notice that when $r_0 = r_1 = \dots = r_d = 1$ the complete *separation of variables* is attained, as the tensor becomes a product of univariate factors. In general we can consider r_1, \dots, r_{d-1} to be larger than 1. In case of two variables, the TT decomposition becomes just a dyadic factorisation of a low-rank matrix. The optimal low-rank matrix approximation can be computed using the singular value decomposition (SVD), and a general TT decomposition can be computed for any tensor by $d-1$ SVDs with quasi-optimal TT ranks for the given accuracy ε [32]. For convenience we can introduce the maximal TT rank $r := \max_{k=1, \dots, d-1} r_k$. Counting the number of unknowns in the TT blocks (2.13), one can conclude that the TT decomposition needs at most dnr^2 unknowns. For numerical efficiency, we assume that r can be taken much smaller than the original cardinality n^d for a desired approximation accuracy.

For theoretical analysis it is convenient to combine (2.13) and (2.11) and consider the *functional* TT format [55],

$$V(\mathbf{x}) \approx \tilde{V}(\mathbf{x}) := \sum_{\alpha_0, \dots, \alpha_d=1}^{r_0, \dots, r_d} v_{\alpha_0, \alpha_1}^{(1)}(x_1) \cdots v_{\alpha_{d-1}, \alpha_d}^{(d)}(x_d),$$

and work directly over the TT ranks of a function. Sharp rank bounds are usually hard to derive though: the SVD might reveal an optimal decomposition that is difficult to express analytically. It was proven in special cases [62, 59, 48] and extensively tested numerically that smooth (e.g. analytic) functions exhibit a logarithmic growth of TT ranks, $r \sim \log^p \varepsilon$, to achieve an error ε . As a rationale for using the TT format for the HJB equations, we show that linear-quadratic value functions admit TT approximations converging at the same rate.

THEOREM 2.2. Assume that the linear system $\dot{\mathbf{y}}(t) = \mathbf{A}\mathbf{y}(t) + \mathbf{B}u$ is stabilisable, i.e. there exists a solution $\Pi \in \mathbb{R}^{d \times d}$ of the Riccati equation

$$A^\top \Pi + \Pi A - \frac{1}{\gamma} \Pi B B^\top \Pi + Q = 0,$$

where Q is a symmetric positive definite matrix with the Cholesky decomposition $Q = D^\top D$, such that the eigenvalues of $A_\pi = AD^{-1} - \frac{1}{\gamma} B B^\top \Pi D^{-1}$ satisfy $\lambda(A_\pi) \in [\lambda_{\min}, \lambda_{\max}] \oplus i[-\mu, \mu]$, $\lambda_{\max} < 0$, and assume that the ranks of the off-diagonal blocks of $A_D = AD^{-1}$ are bounded by a constant, $\text{rank } A_D(k+1:d, 1:k) \leq M$ for all $k = 1, \dots, d-1$, and that $\text{rank}(B) \leq r_b$. Then the value function given by $V(x) = \mathbf{x}^\top \Pi \mathbf{x}$ admits a TT approximation $\tilde{V}(\mathbf{x})$ with the TT rank bound

$$r_k(\tilde{V}) \leq \min \left((M + r_b) \left(\log \frac{1}{\varepsilon} + C \right)^{7/2}, \min(k, d-k) \right) + 2, \quad k = 1, \dots, d-1,$$

and the approximation accuracy $\max_{x \in [-a, a]^d} |V(x) - \tilde{V}(x)| \leq \varepsilon < 1$ for some offset $C = C_0 + C_1 \frac{\mu}{|\lambda_{\max}|} + C_2 \log \left[\frac{\lambda_{\min}}{\lambda_{\max}} \frac{\|A_\pi\| \|D^{-\top} \Pi B\|}{\gamma} \right] > 0$, where C_0, C_1, C_2 are independent of $d, \varepsilon, M, r_b, \gamma, \mu, \lambda_{\min}, \lambda_{\max}$. If the second bound $r_k(\tilde{V}) = \min(k, d-k) + 2$ is attained for all k , the decomposition \tilde{V} is exact.

Proof. For the upper bound we employ [44, Thm 4.2]: for the second order polynomial $V(\mathbf{x}) = \mathbf{x}^\top \Pi \mathbf{x}$ with a symmetric matrix Π there exists an exact TT decomposition with the TT ranks governed by the ranks of the off-diagonal blocks of Π ,

$$(2.14) \quad r_k \leq \text{rank}(\Pi(k+1:d, 1:k)) + 2.$$

This gives an obvious bound $\min(k, d-k) + 2$.

However, there might exist an approximate TT decomposition of lower ranks. First, we notice that the Riccati equation can be rewritten as a Lyapunov equation. In fact, using a stabilised matrix [60] $A - \frac{1}{\gamma} B B^\top \Pi$, and also the Cholesky factor of Q , we obtain

$$(2.15) \quad A_\pi^\top \Pi + \Pi A_\pi = -\frac{1}{\gamma} D^{-\top} \Pi B B^\top \Pi D^{-1} - I,$$

where I is a $d \times d$ identity matrix. The left hand side is constructed from the stable matrix A_π . Using the Kronecker product, we can write the Lyapunov equation as a large linear system,

$$\underbrace{(A_\pi \otimes I + I \otimes A_\pi)}_{\mathcal{A}} \text{vec}(\Pi) = -\frac{1}{\gamma} \sum_{i=1}^{\text{rank}(B)} (D^{-1} \Pi B_i) \otimes (D^{-1} \Pi B_i) - \text{vec}(I),$$

where $\text{vec}(\cdot)$ stacks all columns of a matrix into a vector. Now we can use [48, Thm. 9]: there exists an approximate inverse $\tilde{\mathcal{A}}^{-1}$ of the Kronecker product form

$$\tilde{\mathcal{A}}^{-1} = \sum_{j=-R}^R \frac{2w_j}{\lambda_{\max}} \exp\left(-\frac{2t_j}{\lambda_{\max}} A_\pi\right) \otimes \exp\left(-\frac{2t_j}{\lambda_{\max}} A_\pi\right)$$

with the approximation error

$$(2.16) \quad \|\mathcal{A}^{-1} - \tilde{\mathcal{A}}^{-1}\| \leq \tilde{C} \|\mathcal{A}\| \frac{\sqrt{\lambda_{\min}^2 + \mu^2}}{|\lambda_{\max}|} \exp\left(\frac{2}{\pi} \frac{\mu}{|\lambda_{\max}|} - \pi\sqrt{2R}\right).$$

Multiplying the approximation $\tilde{\mathcal{A}}^{-1}$ with the low-rank first term in the right hand side of (2.15), we obtain an incomplete solution of the form $\text{vec}(\hat{\Pi}) = \sum_{i=1}^{(2R+1)r_b} p_i \otimes q_i$, and hence the rank of $\hat{\Pi}$ is bounded by $(2R+1)r_b$. The negative identity matrix in (2.15) yields the second term

$$(2.17) \quad \text{vec}(\check{\Pi}) = \tilde{\mathcal{A}}^{-1} \text{vec}(-I), \quad \check{\Pi} = \sum_{j=-R}^R -\frac{2w_j}{\lambda_{\max}} \exp\left(-\frac{2t_j}{\lambda_{\max}}(A_\pi + A_\pi^\top)\right)$$

in the ultimate approximate solution $\tilde{\Pi} = \hat{\Pi} + \check{\Pi}$.

Since the first term $\hat{\Pi}$ is a low-rank matrix, all its off-diagonal blocks (2.14) have low ranks of at most $(2R+1)r_b$ too. However, $\check{\Pi}$ is a full-rank matrix and we need to investigate its off-diagonal, also called *quasi-separable* [46], ranks directly. First, we recall [48, Lemma 16] that each matrix exponential in (2.17) can be approximated by a sum of $2k_e + 1$ resolvents with an error

$$(2.18) \quad \left\| \exp\left(-\frac{2t_j}{\lambda_{\max}}(A_\pi + A_\pi^\top)\right) - \sum_{\ell=-k_e}^{k_e} \kappa_\ell \left(z_\ell I + \frac{2t_j}{\lambda_{\max}}(A_\pi + A_\pi^\top)\right)^{-1} \right\| \\ \leq \bar{C} \exp\left(4 \left(\frac{4t_j \mu}{|\lambda_{\max}|} + 1\right)^2 - \left(\frac{4t_j \mu}{|\lambda_{\max}|} + 1\right)^{2/3} k_e^{2/3}\right).$$

Since the quasi-separable rank of $A_{z_\ell} := z_\ell I + \frac{2t_j}{\lambda_{\max}}(A_\pi + A_\pi^\top)$ coincides with that of A_π , which is $M + r_b$, and on the other hand it coincides with the quasi-separable rank of the inverse matrix $A_{z_\ell}^{-1}$ [46, 49], we can conclude that the approximate quasi-separable rank of $\exp\left(-\frac{2t_j}{\lambda_{\max}}(A_\pi + A_\pi^\top)\right)$ is bounded by $(2k_e + 1)(M + r_b)$, and the quasi-separable rank of $\check{\Pi}$ (2.17) is bounded by $(2R+1)(2k_e + 1)(M + r_b)$.

The approximate value function is constructed as $\tilde{V}(\mathbf{x}) = \mathbf{x}^\top \tilde{\Pi} \mathbf{x}$, and by (2.14) we can estimate its TT rank as

$$(2.19) \quad r_k(\tilde{V}) \leq (2R+1)(r_b + (2k_e + 1)(M + r_b)) + 2.$$

For the error estimate, we have

$$\varepsilon = \max_{x \in [-a, a]^d} |V(x) - \tilde{V}(x)| \leq a^2 \|\Pi - \tilde{\Pi}\| \leq a^2 \|\mathcal{A}^{-1} - \tilde{\mathcal{A}}^{-1}\| \left(\frac{\|D^{-\top} \Pi B\|^2}{\gamma} + 1 \right).$$

From (2.16) we obtain

$$R \leq \frac{1}{2\pi^2} \left(\frac{2}{\pi} \frac{\mu}{|\lambda_{\max}|} + \log \|A\| + \log \frac{\sqrt{\lambda_{\min}^2 + \mu^2}}{|\lambda_{\max}|} + \hat{C} + \left| \log \|\mathcal{A}^{-1} - \tilde{\mathcal{A}}^{-1}\| \right| \right)^2, \\ \leq \left(\log \frac{1}{\varepsilon} + \frac{\mu}{|\lambda_{\max}|} + \log \left(\frac{a^2 \|D^{-\top} \Pi B\|^2 \|A_\pi\| \sqrt{\lambda_{\min}^2 + \mu^2}}{\gamma |\lambda_{\max}|} \right) + \hat{C} \right)^2$$

for some constant $\hat{C} > 0$, while (2.18) together with [48, Lemma 5] gives

$$k_e \leq \left(\left| \log \|\mathcal{A}^{-1} - \tilde{\mathcal{A}}^{-1}\| \right| + \log R + \check{C} \right)^{3/2}$$

for $\check{C} > 0$ being some other constant. Plugging these bounds into (2.19), we obtain the first estimate of the TT rank. \square

REMARK 2. In many cases one can take Q , and hence D , to be diagonal matrices, for example, if the 2-norm of the state vector (corresponding to the L^2 -norm of the state function) is used in the cost functional. In this case the ranks of the off-diagonal blocks of A_D coincide with those of A .

REMARK 3. Although Thm. 2.2 is formulated only for linear systems, the remarkable proportionality between the TT ranks of the value function and the off-diagonal ranks of the linearised system matrix seems to hold more generally in practice. In particular, we observe from Fig. 3.3 that the TT ranks of the value function for discretised one-dimensional PDEs grow very mildly with the number of variables, which can be also attributed to the growth of the ratios $\lambda_{\min}/\lambda_{\max}$, μ/λ_{\max} . However, when the system is produced from a two-dimensional PDE, the TT ranks grow proportionally to the number of degrees of freedom introduced in each spatial direction (see Fig. 3.7). Thus, the ranks of the actuator matrix and of the off-diagonal blocks of the Jacobian matrix can give a useful hint whether the TT approach might be efficient for the HJB equation of a particular dynamical system of interest.

REMARK 4. Alternatively, fast convergence of the TT approximation can be related to the smoothness of the original function [62, 59]. For example, it was verified [42] that the cost functional for the bilinear optimal control problem we consider in Sec. 3.2 belongs to $C^\infty(\mathbb{R}^d)$.

2.3.3. TT decomposition of the stiffness matrix and right hand side.

The Galerkin equations (2.12) are still unpractical since they depend on n^d DoFs. In this section we consider how we can decompose the coefficients \mathbf{f} , \mathbf{g} and ℓ into the TT format, and how these decompositions can aid assembling (2.12).

Assuming that the subspace (2.10) is constructed from an orthogonal family, e.g. Legendre polynomials, each coefficient in (2.11) can be written as an integral, which is approximated by a tensorised Gauss-Legendre quadrature, e.g.

$$\mathbf{f}_p(\mathbf{i}) = \int f_p(\mathbf{x}) \Phi_{\mathbf{i}}(\mathbf{x}) d\mathbf{x} \approx \sum_{j_1, \dots, j_d=1}^m w_{j_1} \cdots w_{j_d} f_p(x_{j_1}, \dots, x_{j_d}) \Phi_{i_1, \dots, i_d}(x_{j_1}, \dots, x_{j_d}),$$

where $x_j, w_j, j = 1, \dots, m$, are quadrature nodes on $(-a, a)$ and weights, respectively, and $f_p(\mathbf{x})$ is the p -th component of the drift $\mathbf{f}(\mathbf{x}) = (f_1(\mathbf{x}), \dots, f_d(\mathbf{x}))$, $p = 1, \dots, d$. Suppose that a TT decomposition of $\hat{\mathbf{f}}_p(j_1, \dots, j_d) = f_p(x_{j_1}, \dots, x_{j_d})$ is given,

$$(2.20) \quad \hat{\mathbf{f}}_p(j_1, \dots, j_d) = f_p(x_{j_1}, \dots, x_{j_d}) \approx \sum_{\beta_0, \dots, \beta_d=1}^{R_0, \dots, R_d} \mathbf{f}_{p, \beta_0, \beta_1}^{(1)}(j_1) \cdots \mathbf{f}_{p, \beta_{d-1}, \beta_d}^{(d)}(j_d).$$

Distributing the summations, we can compute all coefficients \mathbf{f}_p in the TT format with a linear cost in d ,

$$(2.21) \quad \mathbf{f}_p(\mathbf{i}) = \sum_{\beta_0, \dots, \beta_d=1}^{R_0, \dots, R_d} \left(\sum_{j_1=1}^m w_{j_1} \phi_{i_1}(x_{j_1}) \mathbf{f}_{p, \beta_0, \beta_1}^{(1)}(j_1) \right) \cdots \left(\sum_{j_d=1}^m w_{j_d} \phi_{i_d}(x_{j_d}) \mathbf{f}_{p, \beta_{d-1}, \beta_d}^{(d)}(j_d) \right).$$

Similarly we can compute the right hand side tensor $\mathbf{b}(\mathbf{i}) = \langle \Phi_{\mathbf{i}}(\mathbf{x}), \ell(\mathbf{x}) + \gamma \check{u}(\mathbf{x})^2 \rangle_{L^2(\Omega)}$.

Matrices of size $n^d \times n^d$ can be represented in a slightly different *matrix* TT format, where we separate pairs of row and column indices,

$$(2.22) \quad A(\mathbf{i}, \mathbf{j}) = \sum_{\beta_0, \dots, \beta_d=1}^{R_0, \dots, R_d} A_{\beta_0, \beta_1}^{(1)}(i_1, j_1) \cdots A_{\beta_{d-1}, \beta_d}^{(d)}(i_d, j_d).$$

For cost estimates we define also the upper bound $R \geq R_k$, $k = 0, \dots, d$. Combining (2.20) and (2.12), we can decompose the linear part of the stiffness matrix as follows,

$$A_{f_p}(\mathbf{i}, \mathbf{j}) := \langle \Phi_{\mathbf{i}}, f_p D_p \Phi_{\mathbf{j}} \rangle_{L^2(\Omega)} = \sum_{\beta_0, \dots, \beta_d=1}^{R_0, \dots, R_d} A_{p, \beta_0, \beta_1}^{(1)}(i_1, j_1) \cdots A_{p, \beta_{d-1}, \beta_d}^{(d)}(i_d, j_d),$$

where

$$(2.23) \quad A_{p, \beta_{p-1}, \beta_p}^{(p)}(i_p, j_p) = \left(\sum_{k_p=1}^m w_{k_p} \phi_{i_p}(x_{k_p}) \mathbf{f}_{p, \beta_{p-1}, \beta_p}^{(p)}(k_p) \frac{d\phi_{j_p}(x_{k_p})}{dx} \right),$$

and

$$(2.24) \quad A_{p, \beta_{q-1}, \beta_q}^{(q)}(i_q, j_q) = \left(\sum_{k_q=1}^m w_{k_q} \phi_{i_q}(x_{k_q}) \mathbf{f}_{p, \beta_{q-1}, \beta_q}^{(q)}(k_q) \phi_{j_q}(x_{k_q}) \right)$$

for $q \neq p$. Summing all different components A_{f_p} , one obtains the complete linear part $\langle \Phi_{\mathbf{i}}, \mathbf{f}^\top D \Phi_{\mathbf{j}} \rangle_{L^2(\Omega)}$. This summation can be performed in the TT format directly, followed by a rank truncation [32], or using the iterative Alternating Linear Scheme approximation (see Sec. 2.3.4 and [51]).

The system functions are approximated in the TT format (2.20) using another iterative procedure, the so-called *TT-Cross* algorithm [57]. Any exact TT decomposition, e.g. (2.20), can be recovered from samples of the original tensor by an *interpolation formula* [58]

$$(2.25) \quad \hat{\mathbf{f}}_p(\mathbf{i}) = \sum_{\substack{\beta_k, \beta'_k=1 \\ k=1, \dots, d-1}}^{R_k} \hat{\mathbf{f}}_p(i_1, \mathcal{I}_{\beta_1}^{>1}) \left(\hat{\mathbf{f}}_p(\mathcal{I}^{\leq 1}, \mathcal{I}^{>1}) \right)_{\beta'_1, \beta_1}^{-1} \hat{\mathbf{f}}_p(\mathcal{I}_{\beta_1}^{\leq 1}, i_2, \mathcal{I}_{\beta_2}^{>2}) \cdots \hat{\mathbf{f}}_p(\mathcal{I}_{\beta_{d-1}}^{\leq d-1}, i_d),$$

where $\mathcal{I}^{\leq k} = \{i_1^{\beta_1}, \dots, i_k^{\beta_k}\}_{\beta_k=1}^{R_k}$ and $\mathcal{I}^{> k} = \{i_{k+1}^{\beta_{k+1}}, \dots, i_d^{\beta_d}\}_{\beta_k=1}^{R_k}$ are *left*, respectively, *right* index sets chosen such that the intersection matrices $\hat{\mathbf{f}}_p(\mathcal{I}^{\leq k}, \mathcal{I}^{> k})$ are invertible. For uniformity of notation, we let $\mathcal{I}^{\leq 0} = \mathcal{I}^{> d} = \emptyset$. Note that the inverse intersection matrices can be multiplied with the adjacent three-dimensional factors to obtain the TT blocks (2.13), e.g. $\mathbf{f}_{\beta_{k-1}, \beta_k}^{(k)}(i_k) = \sum_{\beta'_k} \hat{\mathbf{f}}_p(\mathcal{I}_{\beta_{k-1}}^{\leq k-1}, i_k, \mathcal{I}_{\beta'_k}^{> k}) \left(\hat{\mathbf{f}}_p(\mathcal{I}^{\leq k}, \mathcal{I}^{> k}) \right)_{\beta'_k, \beta_k}^{-1}$. For numerical stability, the inversion is computed via the QR decomposition [57] or the incremental LU decomposition [58].

In practice, one seeks an approximate decomposition of the form (2.25). In this case it becomes important to find indices that not only give invertible intersection matrices, but deliver a small approximation error. The TT-Cross algorithm optimises the index positions iteratively. In the first step, assume that the right sets $\mathcal{I}^{> k}$ are given (for example at random). One can compute the first factor $F^{\{1\}}(i_1, \beta_1) = \hat{\mathbf{f}}_p(i_1, \mathcal{I}_{\beta_1}^{>1})$, which can be seen as an $m \times R_1$ matrix. The smallest approximation error among sampling rank- R_1 approximations is given by such $i_1 \in \mathcal{I}^{\leq 1} \subset \{1, \dots, m\}$ that select the submatrix of maximum volume, i.e. $|\det F^{\{1\}}(\mathcal{I}^{\leq 1}, :)| = \max_{\#\mathcal{I}=R_1} |\det F^{\{1\}}(\mathcal{I}, :)|$. This set can be found by the *maxvol* algorithm [47] in $\mathcal{O}(mR_1^2)$ operations, similarly to the LU decomposition with pivoting.

Assume now that we have the left index set $\mathcal{I}^{\leq k-1}$ and the right set $\mathcal{I}^{> k}$. We can compute $R_{k-1}mR_k$ elements of the tensor and arrange them as a $R_{k-1}m \times R_k$ matrix

with elements $F^{\{k\}}(\beta_{k-1}i_k, \beta_k) = \hat{\mathbf{f}}_p(\mathcal{I}_{\beta_{k-1}}^{\leq k-1}, i_k, \mathcal{I}_{\beta_k}^{>k})$. Now we can apply the `maxvol` algorithm to $F^{\{k\}}$ to derive the next index set $\mathcal{I}^{\leq k}$ as a subset of the union of $\mathcal{I}^{\leq k-1}$ and i_k . This recursive procedure continues until the last TT block $\hat{\mathbf{f}}_p(\mathcal{I}^{\leq d-1}, i_d)$ is computed. Moreover, we can reverse it in a similar fashion and carry out several TT-Cross iterations, as shown in Algorithm 2.2. This allows to optimise all index sets and, consequently, the approximations (2.25), (2.20) even if the initial guess was inaccurate.

Algorithm 2.2 TT-Cross iteration

- 1: Pick initial sets $\mathcal{I}^{>k} \in \mathbb{N}^{r_k \times d-k}$, $k = 1, \dots, d-1$.
 - 2: **for** $k = 1, 2, \dots, d$ **do**
 - 3: Evaluate $r_{k-1}mr_k$ elements $F^{\{k\}}(\beta_{k-1}i_k; \beta_k) := \hat{\mathbf{f}}_p(\mathcal{I}_{\beta_{k-1}}^{\leq k-1}, i_k, \mathcal{I}_{\beta_k}^{>k})$.
 - 4: Apply `maxvol` algorithm to $F^{\{k\}}$ to obtain $\mathcal{I}^{\leq k} \subset \mathcal{I}^{\leq k-1} \cup \{i_k\}$.
 - 5: **end for**
 - 6: **for** $k = d, d-1, \dots, 2$ **do**
 - 7: Evaluate $r_{k-1}mr_k$ elements $F^{\{k\}}(\beta_{k-1}; i_k\beta_k) := \hat{\mathbf{f}}_p(\mathcal{I}_{\beta_{k-1}}^{\leq k-1}, i_k, \mathcal{I}_{\beta_k}^{>k})$.
 - 8: Apply `maxvol` algorithm to $(F^{\{k\}})^\top$ to obtain $\mathcal{I}^{>k-1} \subset \{i_k\} \cup \mathcal{I}^{>k}$.
 - 9: **end for**
 - 10: Assemble TT blocks $\mathbf{f}_{\beta_{k-1}, \beta_k}^{(k)}(i_k) = \sum_{\beta'_k} \hat{\mathbf{f}}_p(\mathcal{I}_{\beta_{k-1}}^{\leq k-1}, i_k, \mathcal{I}_{\beta'_k}^{>k}) (\hat{\mathbf{f}}_p(\mathcal{I}^{\leq k}, \mathcal{I}^{>k}))^{-1}_{\beta'_k, \beta_k}$.
-

REMARK 5. *The result of TT-Cross might still depend on the heuristically chosen initial indices. Therefore, we distinguish the stopping threshold (called δ from now on) and the actual approximation error ε in the rest of the paper.*

Having computed TT approximations to all components f_p , we construct the matrix TT blocks (2.23)–(2.24). Similarly, we apply the TT-Cross algorithm to construct all components of $\mathbf{g}\check{u}$, assemble the corresponding parts of the stiffness matrix (2.12) in the TT format, and sum them together.

We can also precompute a TT matrix of the form (2.22) which maps the value function coefficients into the tensor of $\check{u}(\mathbf{x})$ values on the quadrature grid. In the unconstrained control case, we have that $\check{u} = -\frac{1}{2\gamma} \mathbf{g}^\top D\check{V}$, and hence we assemble

$$\hat{B}(\mathbf{j}, \mathbf{i}) = \sum_{p=1}^d \sum_{\beta_0, \dots, \beta_d} -\frac{1}{2\gamma} \left(\mathbf{g}_{p, \beta_0, \beta_1}^{(1)}(j_1) \phi_{i_1}^{\delta(p,1)}(x_{j_1}) \right) \cdots \left(\mathbf{g}_{p, \beta_{d-1}, \beta_d}^{(d)}(j_d) \phi_{i_d}^{\delta(p,d)}(x_{j_d}) \right),$$

using the TT approximations of $g_p(\mathbf{x})$, where

$$\phi_i^{\delta(p,q)} = \begin{cases} d\phi_i/dx, & p = q, \\ \phi_i, & \text{otherwise.} \end{cases}$$

Now the control signal $\check{u} \approx \hat{B}\check{\mathbf{v}}$ can be constructed simply as a sum of products of a TT matrix (2.22) and a TT tensor (2.13) with $\mathcal{O}(d^2n^2R^2r^2)$ complexity [32]. In the constrained control case, the first step is the same, followed by approximating the pointwise constraint function

$$(2.27) \quad \check{u}(i_1, \dots, i_d) = \check{u}_{\max} \tanh((\hat{B}\check{\mathbf{v}})(i_1, \dots, i_d)/\check{u}_{\max})$$

in the TT format using again the TT-Cross method. Since the TT approximation may over- or undershoot the exact limits by the relative approximation error $\varepsilon \leq \delta$, we seek a slightly tighter bound $\tilde{u}_{\max} = (1 - \delta)u_{\max}$.

2.3.4. The iterative method for the solution of the nonlinear system.

The policy update solves (2.12) at every iteration by taking the previous iterate of the value tensor $\tilde{\mathbf{v}}$, constructing the control signal, the stiffness matrix and the right hand side, and finally by solving the linear system on the new value tensor approximation.

The latter step implies using only iterative methods that can preserve the TT structure of all data. The simplest strategy would be to implement traditional iterative methods (e.g. GMRES) with TT matrix-vector operations and rank truncation [53, 52, 40]. However, the TT ranks of auxiliary (e.g. Krylov) vectors may become very high unless a very good preconditioner exists. Therefore, we switch to a more robust technique used nowadays, the Alternating Linear Scheme (ALS) [51].

The ALS is a linear projection method similarly to the Krylov techniques, but in contrast to the latter it projects the equations onto bases constructed from the TT decomposition of the solution itself. Notice that the TT decomposition (2.13) is linear with respect to the elements of each particular TT block, e.g. $\mathbf{v}^{(k)}$. Given (2.13), let us define a partial TT decomposition where $\mathbf{v}^{(k)}$ is replaced by the identity matrix,

$$(2.28) \quad \begin{aligned} V_{\neq k}(i_1, \dots, i_d; \alpha_{k-1}, j_k, \alpha_k) = & \sum_{\substack{\alpha_0, \dots, \alpha_{k-2}, \\ \alpha_{k+1}, \dots, \alpha_d}} \mathbf{v}_{\alpha_0, \alpha_1}^{(1)}(i_1) \cdots \mathbf{v}_{\alpha_{k-2}, \alpha_{k-1}}^{(k-1)}(i_{k-1}) \\ & \cdot \delta(i_k, j_k) \\ & \cdot \mathbf{v}_{\alpha_k, \alpha_{k+1}}^{(k+1)}(i_{k+1}) \cdots \mathbf{v}_{\alpha_{d-1}, \alpha_d}^{(d)}(i_d). \end{aligned}$$

Clearly, the original TT decomposition (2.13) can be produced from $V_{\neq k}$ by just multiplying it with the k -th TT block. Specifically, we introduce the vector form

$$(2.29) \quad \bar{v}^{(k)}(\alpha_{k-1}, i_k, \alpha_k) = \mathbf{v}_{\alpha_{k-1}, \alpha_k}^{(k)}(i_k), \quad \bar{v}^{(k)} \in \mathbb{R}^{r_{k-1} n_k r_k},$$

and treat $V_{\neq k}$ as a $n^d \times (r_{k-1} n_k r_k)$ matrix. One can check that

$$\tilde{\mathbf{v}} = V_{\neq k} \bar{v}^{(k)}$$

holds for any $k = 1, \dots, d$.

Now, assuming that the entire stiffness matrix $A = \left[\langle \Phi_{\mathbf{i}}, (\mathbf{f} + \mathbf{g}\ddot{u})^\top D\Phi_{\mathbf{j}} \rangle_{L^2(\Omega)} \right]_{\mathbf{i}, \mathbf{j}}$ and the right hand side $\mathbf{b} = \left[-\langle \Phi_{\mathbf{i}}, \ell + \gamma \ddot{u}^2 \rangle_{L^2(\Omega)} \right]_{\mathbf{i}}$ in (2.12) are assembled in TT formats (2.22) and (2.13), the ALS method iterates over $k = 1, \dots, d$ (hence the name alternating), seeking for one TT block at a time by making the residual orthogonal to $V_{\neq k}$,

$$(2.30) \quad (V_{\neq k}^\top A V_{\neq k}) \bar{v}^{(k)} = (V_{\neq k}^\top \mathbf{b}).$$

Notice that the reduced system (2.30) is of size $r_{k-1} n_k r_k$, i.e. much smaller than the original system (2.12). Once we solve (2.30), we populate the TT block $\mathbf{v}^{(k)}$ with the elements of $\bar{v}^{(k)}$ through (2.29), and use the updated $\mathbf{v}^{(k)}$ to construct (2.28) in the next step $k \rightarrow k + 1$ or $k \rightarrow k - 1$. Efficient practical implementation employs the fact that (2.28) mimics the original TT decomposition (2.13) in the sense that same original indices i_1, \dots, i_d are separated. Therefore, given (2.22), the reduced

matrix $V_{\neq k}^\top A V_{\neq k}$ can be computed block by block in a total of $\mathcal{O}(dn^2r^4)$ operations [51, 56]. Here we assume also that $R = \mathcal{O}(r)$, which is the case for the quadratic HJB equation. Since the reduced matrix in (2.30) inherits the low-rank structure of the matrix TT decomposition (2.22), we can solve (2.30) iteratively using a fast matrix-vector product with the same cost of $\mathcal{O}(dn^2r^4)$. The TT blocks can also be enriched with auxiliary vectors, such as approximate residuals [45], which gives a mechanism for increasing TT ranks and adapting them to the desired accuracy. Consider an auxiliary TT decomposition approximating the residual, projected onto the first $k-1$ TT blocks of the solution,

$$(\mathbf{b} - A\mathbf{v})(i_1, \dots, i_d) \approx \sum_{\alpha_0, \dots, \beta_d=1}^{r_0, \dots, \rho_d} \mathbf{v}_{\beta_0, \beta_1}^{(1)}(i_1) \cdots \mathbf{v}_{\alpha_{k-2}, \alpha_{k-1}}^{(k-1)}(i_{k-1}) \\ \cdot \mathbf{z}_{\alpha_{k-1}, \beta_k}^{(k)}(i_k) \cdot \mathbf{z}_{\beta_k, \beta_{k+1}}^{(k+1)}(i_{k+1}) \cdots \mathbf{z}_{\beta_{d-1}, \beta_d}^{(d)}(i_d).$$

After solving (2.30) and updating (2.29), we expand $\mathbf{v}^{(k)}$ and $\mathbf{v}^{(k+1)}$ increasing their ranks by ρ_k ,

$$(2.31) \quad \mathbf{v}^{(k)}(i_k) := [\mathbf{v}^{(k)}(i_k) \quad \mathbf{z}^{(k)}(i_k)], \quad \mathbf{v}^{(k+1)}(i_{k+1}) := \begin{bmatrix} \mathbf{v}^{(k+1)}(i_{k+1}) \\ 0 \end{bmatrix}.$$

Note that this step does not perturb the whole solution tensor $\tilde{\mathbf{v}}$ due to the zero block in $\mathbf{v}^{(k+1)}$, but the subspace of columns of $V_{\neq k+1}$ in the next step is enriched due to the residual block $\mathbf{z}^{(k)}$. To reduce the TT rank, we can truncate $\mathbf{v}^{(k)}$ using the SVD.

Finally, we can *orthogonalise* TT blocks using QR decompositions [32] such that

$$(2.32) \quad \sum_{\alpha_{k-1} i_k} \mathbf{v}_{\alpha_{k-1}, \alpha_k}^{(k)}(i_k) \mathbf{v}_{\alpha_{k-1}, \beta_k}^{(k)}(i_k) = \delta(\alpha_k, \beta_k)$$

or

$$(2.33) \quad \sum_{i_k \alpha_k} \mathbf{v}_{\alpha_{k-1}, \alpha_k}^{(k)}(i_k) \mathbf{v}_{\beta_{k-1}, \alpha_k}^{(k)}(i_k) = \delta(\alpha_{k-1}, \beta_{k-1}).$$

This makes the projection matrix $V_{\neq k}$ orthogonal as well, which improves numerical stability of the algorithm.

If the matrix A was symmetric positive definite then the projected system (2.30) could be rigorously related to the energy optimization problem and the nonlinear block Gauss–Seidel method. In our problem (2.12) this is not the case: A is non-symmetric and degenerate due to the gradient operator D , which annihilates any constant component in the solution. In this case, the degenerate reduced matrix in (2.30) can prevent convergence.

However, A is compatible with the right hand side under the condition $\ell(0) = \tilde{u}(0) = 0$. Moreover, the eigenvalues of A are located in the right half of the complex plane for a suitable choice of the domain size a and polynomial order n . In this case we can resolve both issues by solving shifted systems, mimicking the implicit Euler time propagation. We introduce a shift $\mu > 0$, and solve

$$(2.34) \quad (A + \mu I) \mathbf{v} = \mathbf{b} + \mu \tilde{\mathbf{v}},$$

where $\tilde{\mathbf{v}}$ is the previous iterate of \mathbf{v} . In practice, we can even combine (2.34) and the policy updates (2.9) into the single iteration, as shown in Algorithm 2.3.

Algorithm 2.3 Policy update with the adaptive ALS iteration

-
- 1: Choose initial value tensor \mathbf{v} , shift $\mu > 0$, stopping threshold $\delta > 0$, $\check{\mathbf{v}} = 0$.
 - 2: **while** $\|\mathbf{v} - \check{\mathbf{v}}\|_2 > \delta \|\mathbf{v}\|_2$ **do** {Policy iteration}
 - 3: Update $\check{\mathbf{v}} = \mathbf{v}$ and (optionally) $\mu := \mu q$ for some $0 < q < 1$.
 - 4: Compute the control \check{u} using (2.26) and (optionally) (2.27).
 - 5: Construct $A[\check{u}]$ and $\mathbf{b}[\check{u}]$ for (2.12) using Alg. 2.2 and (2.22)–(2.24).
 - 6: Orthogonalise TT blocks of \mathbf{v} s.t. (2.33) holds.
 - 7: **for** $k = 1, \dots, d$ **do** {ALS algorithm}
 - 8: Assemble and solve $(V_{\neq k}^\top A V_{\neq k} + \mu I) \bar{v}^{(k)} = V_{\neq k}^\top \mathbf{b} + \mu V_{\neq k}^\top \check{\mathbf{v}}$ using (2.28).
 - 9: Update $\mathbf{v}^{(k)}$ via (2.29) and truncate r_k using SVD up to accuracy δ .
 - 10: Enrich $\mathbf{v}^{(k)}, \mathbf{v}^{(k+1)}$ using (2.31) and orthogonalise s.t. (2.32) holds.
 - 11: **end for**
 - 12: **end while**
-

If $\operatorname{Re} \lambda(A) \geq 0$, then the spectral radius of the transition matrix $\mu(A + \mu I)^{-1}$ is less than 1 for any $\mu > 0$. On the other hand, if $\mu > -\mathbf{v}^\top A \mathbf{v}$ for any $\mathbf{v} : \|\mathbf{v}\|_2 = 1$, then the reduced matrix $V_{\neq k}^\top A V_{\neq k} + \mu I$ (remember that $V_{\neq k}^\top V_{\neq k} = I$) is invertible. This gives a freedom to choose μ such that the method remains stable and converges fast enough. In practice we need to ensure $\mu > -\mathbf{v}^\top A \mathbf{v}$ only for those \mathbf{v} that belong to span $V_{\neq k}$. It turns out that as the solution converges, we can decrease μ geometrically (in particular, we multiply it by a factor $q = 0.98$ in each iteration), which ensures faster convergence near the end of the process.

3. Optimal Feedback Control of PDEs. In the following, we illustrate how the presented framework sets the grounds for developing a computational approach for the synthesis of optimal feedback controllers for high-dimensional nonlinear dynamical systems. In particular, we focus on the class of nonlinear parabolic PDEs including nonlinear reaction-diffusion equations and bilinear control problems with Fokker-Planck dynamics. While the continuous dynamics are infinite-dimensional, semi-discretization in space via finite elements or spectral methods leads to high-dimensional nonlinear control systems where the optimal synthesis problem can be addressed within the methodology presented in this paper².

3.1. The Newell-Whitehead equation. We consider the following nonlinear diffusion-reaction equation [21]:

$$(3.1) \quad \begin{aligned} \partial_t x(\xi, t) &= \sigma \partial_{\xi\xi} x + x(1 - x^2) + \chi_\omega(\xi) u(t) \quad \text{in } [-1, 1] \times \mathbb{R}^+, \\ \partial_\xi x(-1, t) &= \partial_\xi x(1, t) = 0, \quad t \in \mathbb{R}^+, \\ x(\xi, 0) &= 2 + \cos(2\pi\xi) \cos(\pi\xi). \end{aligned}$$

This equation has 0 as unstable equilibrium and ± 1 as stable equilibria. We take the diffusion coefficient $\sigma = 0.2$, the control is applied on a subdomain $\omega = [-0.5, 0.2]$, and the running cost is

$$(3.2) \quad \mathcal{J}(u, x) = \int_0^\infty \|x(\xi, t)\|_{L_2(-1,1)}^2 + \gamma u(t)^2 dt,$$

²All tests were carried out in Matlab 2017b on one core of an Intel Xeon E5-2640 v4 CPU at 2.4 GHz.

where for concreteness we take $\gamma = 0.1$. Thus, the control objective consists in stabilizing the unstable equilibrium. The PDE (3.1) is discretized by Chebyshev pseudospectral collocation method [61] using d points $\xi_k = -\cos(\pi k/d)$, $k = 1, \dots, d$. The discrete state can thus be collected into a vector of nodal values $X(t) = (X_1(t), \dots, X_d(t))$ where $X_k(t) \approx x(\xi_k, t)$. This gives us a d -dimensional nonlinear ODE

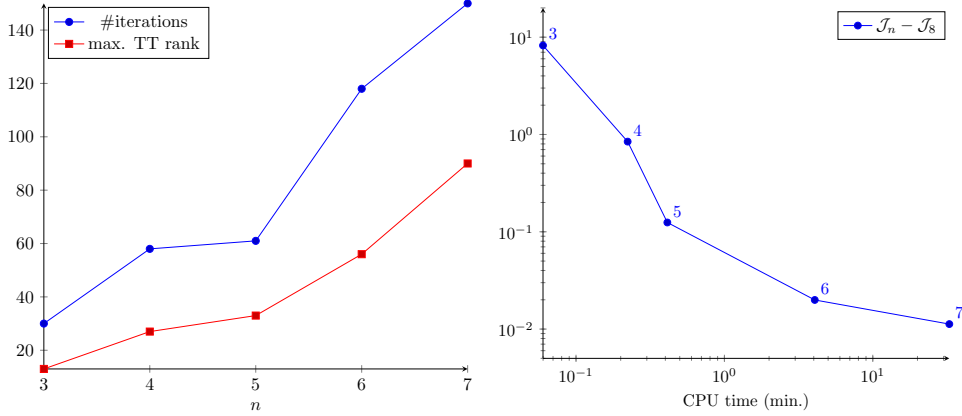
$$(3.3) \quad \frac{dX}{dt} = AX + X \odot (1 - X \odot X) + Bu(t),$$

where “ \odot ” is the Hadamard product, A is the pseudospectral differentiation matrix corresponding to the Laplace operator, and B is a vector corresponding to the pseudospectral discretisation of the indicator function $\chi_\omega(\xi)$ of the subdomain ω .

The HJB equation solver is applied directly to (3.3), restricting the domain of the value function to $(-3, 3)^d$, and the LQR method uses the matrix of (3.3) linearised at the origin, $A_L = A + I$. Once the value function (or LQR coefficients) is obtained, the controlled ODE is solved using the `ode15s` Runge-Kutta method with a relative accuracy tolerance 10^{-6} , and the running cost (3.2) is approximated by the trapezoidal rule on the time points produced by `ode15s`.

First, we investigate the performance of the TT scheme with respect to the approximation parameters, the number of Legendre polynomials n in each variable (Fig. 3.1) and the stopping threshold δ in Alg. 2.3 (Fig. 3.2). Moreover, we vary the number of variables d , i.e. the number of spatial discretisation points for the PDE model (Fig. 3.3). The initial offset in (2.34) is set to $\mu = 50$.

Fig. 3.1: Numbers of policy iterations and maximal TT ranks (left); differences in total running cost and CPU times (right) for different univariate polynomial degrees n . Numbers above points in the right plot denote n . Other settings $\delta = 10^{-3}$ and $d = 14$.



Due to the nonlinearity in (3.3), the value function is significantly far from a quadratic polynomial, which is reflected in Fig. 3.1 by the linear growth of TT ranks with n , and a relatively slow algebraic decay of the error (cf. Remark 1). Nevertheless, even an order-4 approximation can give a substantially better control signal than the quadratic approximation, see Fig. 3.4. From Fig. 3.2 we see that the number of iterations and the TT ranks depend logarithmically on the TT approximation error, which is a more optimistic result than that predicted by Thm. 2.2, although the problem is nonlinear. The errors in the total cost start higher than the threshold δ , but eventually the two error indicators are of the same order.

Fig. 3.2: Numbers of policy iterations and maximal TT ranks (left); differences in total running cost and CPU times (right) for different TT approximation thresholds δ . Numbers above points in the right plot denote δ . Other settings $n = 5$ and $d = 14$.

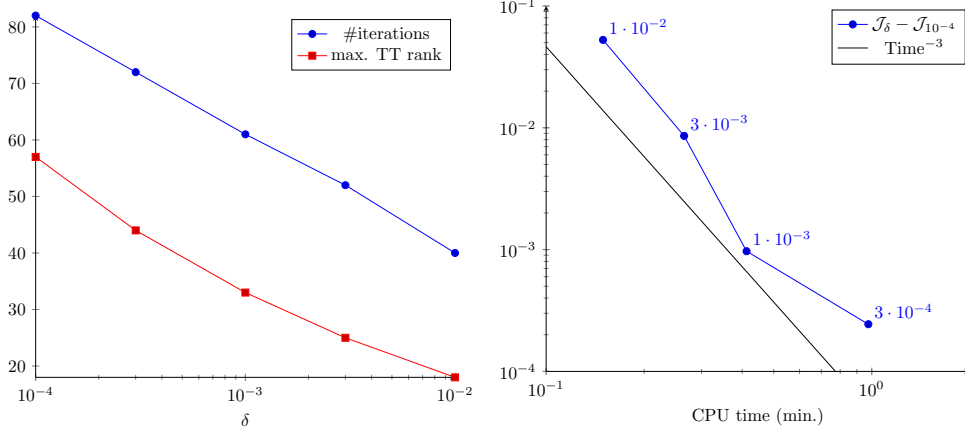


Fig. 3.3: Numbers of policy iterations and maximal TT ranks (left); differences in total running cost and CPU times (right) for different spatial dimensions d . Numbers above points in the right plot denote d . Other settings $n = 5$ and $\delta = 10^{-3}$.

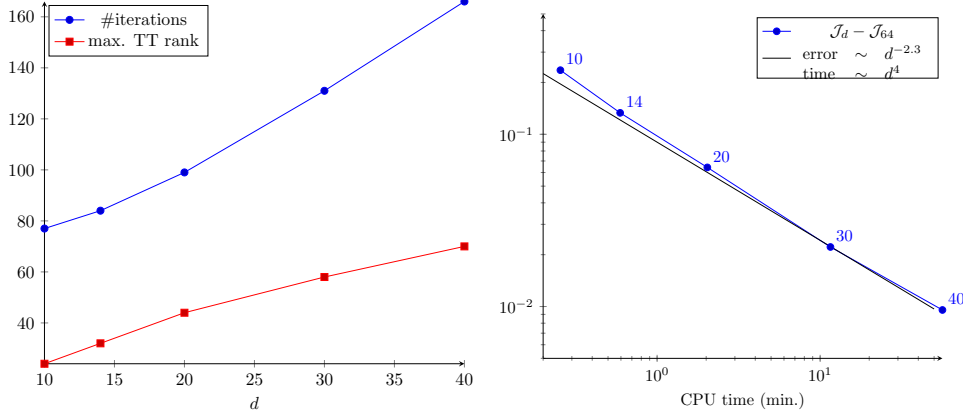
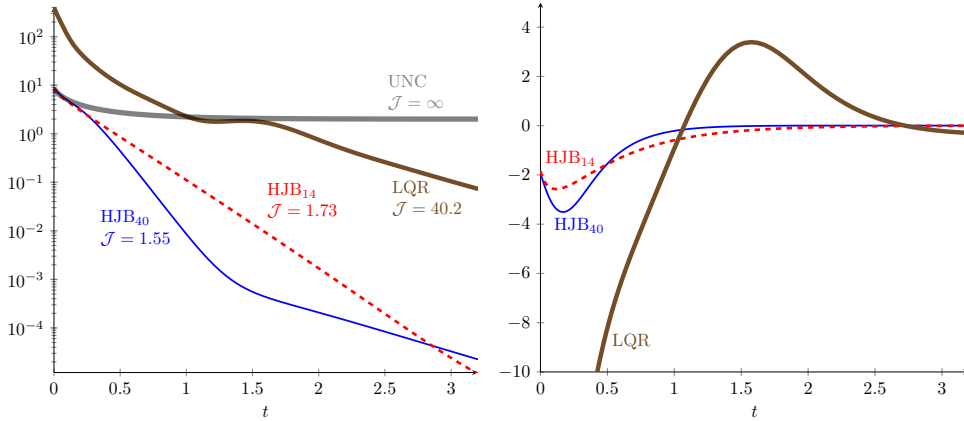


Fig. 3.3 investigates the performance with respect to the dimension. The maximal TT rank grows linearly with the dimension, and the $\mathcal{O}(dn^2r^4)$ complexity of the ALS method implies the total cost bound in order of d^5 . The practical cost is closer to $\mathcal{O}(d^4)$ which might be attributed to non-uniform distribution of TT ranks along the decomposition. This is a significant reduction compared to the exponential cost of the full Cartesian ansatz. However, the method might still become slow in very high dimensions, mainly due to the increase in the number of policy iterations, resulting from a larger condition number of the linearised system. A possible remedy is to construct the value function for a lower-dimensional discretisation of the PDE, and interpolate the state of a system with finer discretisation onto this lower-dimensional spatial grid. This would yield a suboptimal control of course, but the error should be

proportional to the discretisation error of the lower-dimensional grid, which might be much smaller than the error resulting from the linearization of the system.

Fig. 3.4: Time evolution of running costs (left) and control signals (right) for the Newell-Whitehead problem (3.1) with $d = 40$.

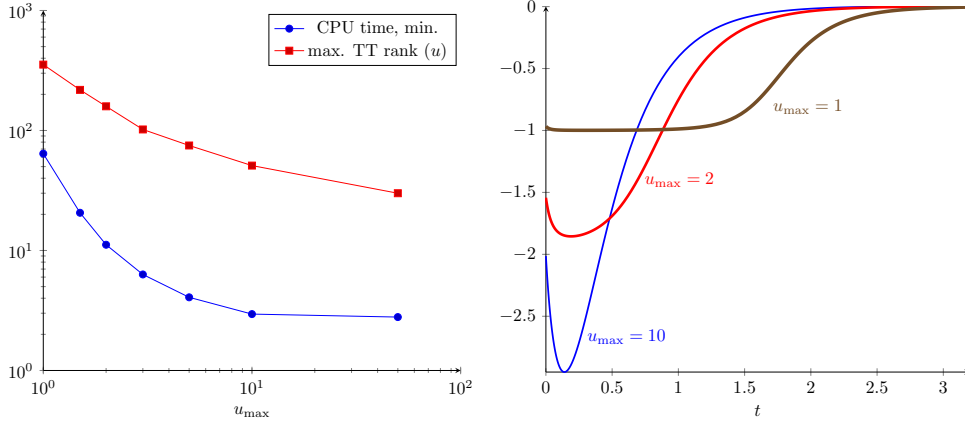


In Fig. 3.4 (left) we plot the running costs for the HJB regulator for the system dimension 40 with $n = 5$ and $\delta = 10^{-3}$ (HJB₄₀), an interpolated regulator from dimension 14 and the same $n = 5, \delta = 10^{-3}$ (HJB₁₄), an LQR regulator for the given system, and finally the cost of the UNControlled system (both with $d = 40$). Fig. 3.4 (right) shows the corresponding control signals. Since the linearized system is unstable, the LQR computes a very strong control at the beginning. The HJB is able to detect the stabilizing nonlinearity and produce a control at much lower cost. Moreover, the low-dimensional value function can be a good approximation for a high-dimensional system, with only a slight overhead in the cost. Note that the uncontrolled state converges to $X = 1$ with an infinite undiscounted cost.

Newell-Whitehead problem with control constraints. Often constrained state or control are of interest. The constraints might stem from physical properties of the solution (e.g. non-negativity), or the actuator (e.g. maximal possible force). Fig. 3.5 shows the total CPU times and TT ranks of the constrained control (2.27), as well as the control signals for three limiting parameters. Since the tanh function becomes more kinky for more severe constraints, the TT ranks increase which slows down the computations. Nevertheless, it is possible to adjust the value function to the constraint using the ALS policy update algorithm.

Newell-Whitehead problem with 2-dimensional space. Next, we consider an extension of the problem (3.1) to two spatial dimensions, i.e. where the state depends on two space coordinates, $x(\boldsymbol{\xi}, t) = x(\xi_1, \xi_2, t)$. We replace the second derivative with the Laplace operator, and the control is applied on the domain $\omega = [-0.5, 0.2]^2$. We use the Cartesian product of the same Chebyshev grids in each direction, and similar homogeneous Neumann conditions on the boundary of $\Omega = [-1, 1]^2$. The performance of the TT-HJB controller is tested on the initial state $x(\boldsymbol{\xi}, 0) = 2 + \cos(2\pi\xi_1)\cos(\pi\xi_2)$. In Fig. 3.6 we can see that again the magnitude of the HJB-controlled state is much smaller than that controlled with LQR for the same transient time.

Fig. 3.5: CPU times and TT ranks (left) and control signals (right) for different control constraints $-u_{\max} \leq u \leq u_{\max}$ in the Newell-Whitehead problem.



The CPU times and TT ranks are shown in Fig. 3.7 (left). Although Theorem 2.2 is not immediately applicable to a nonlinear system, we still observe a linear growth of the TT ranks with the number of Chebyshev points in each direction \sqrt{d} . The absolute values of the ranks are larger than those in the one-dimensional case, which leads to significant computing times. On the other hand, Fig. 3.7 (right) indicates that the discretisation is still insufficient: switching from 9 to 11 Chebyshev points in each direction affects the control signal considerably. For higher-dimensional problems it might be reasonable to reduce the model first. In the next section we employ a generalization of the balanced truncation method to bilinear systems [41] for this purpose.

Fig. 3.6: State snapshots at $t = 0.6$ in the Newell-Whitehead problem with two spatial coordinates with HJB (left) and LQR (right) controllers.

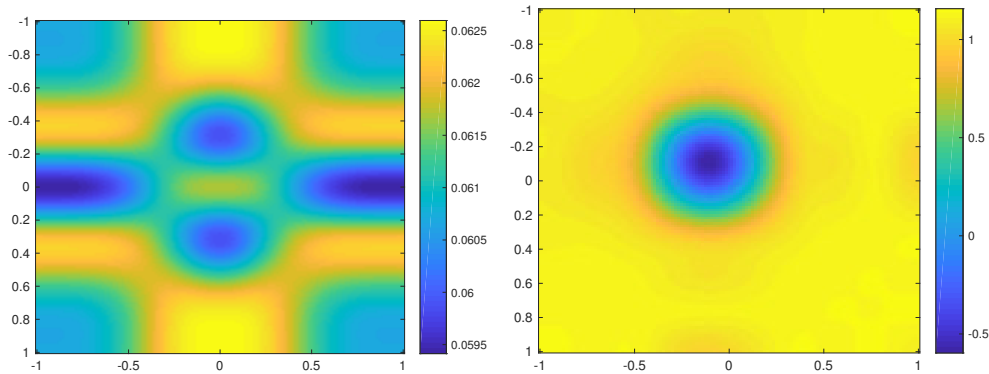
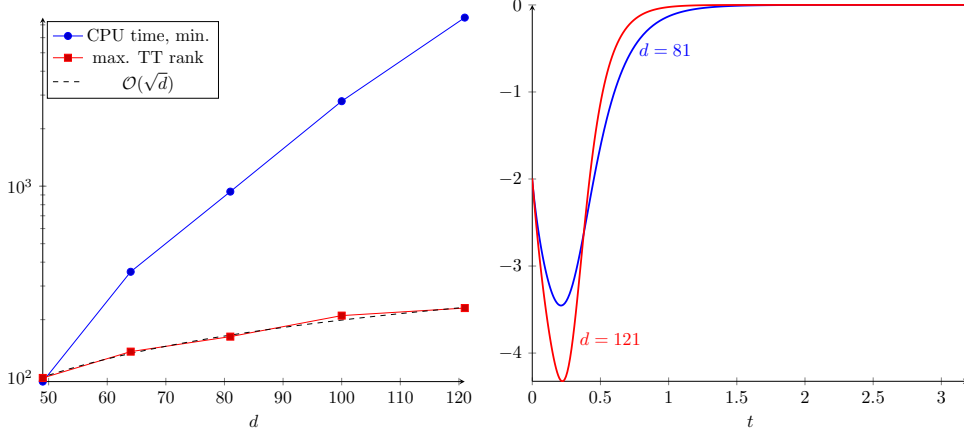


Fig. 3.7: CPU times and TT ranks (left) and control signals (right) for different spatial dimensions d in the Newell-Whitehead problem with two spatial coordinates.



3.2. The Fokker-Planck equation. In this section we compute regulators for the stabilised bilinearly controlled Fokker-Planck equation

$$(3.4) \quad \begin{aligned} \partial_t x(\xi, t) &= \nu \partial_{\xi\xi} x + \partial_{\xi}(x \partial_{\xi} G) + u \partial_{\xi}(x \partial_{\xi} H), \quad \xi \in \Omega, \\ 0 &= [\partial_{\xi} x + x \partial_{\xi}(G + uH)]|_{\xi \in \partial\Omega}, \end{aligned}$$

where the computational domain will be set $\Omega = (-6, 6)$. This equation models the density of particles, controlled with laser-induced electric force with potential $G(x) + u(t)H(x)$ [50], with G the ground and H the control potential. This system has 0 as an eigenvalue with associated eigenstate $x_{\infty} = \exp(-(\log \nu + \frac{G}{\nu}))$, see eg. [43]. Henceforth the eigenstates are considered as normalized in $L^2(\Omega)$. It is known that x_{∞} is stable, but the convergence to this steady state, which is given by the second eigenvalue and depends on ν and G , can be extremely slow, see for instance [54, pg 251]. Thus, to speed up convergence in the transient phase, control is of importance. To obtain a suitable stabilization problem we introduce the shifted state $y = x - x_{\infty}$. It satisfies

$$(3.5) \quad \begin{aligned} \partial_t y(\xi, t) &= \nu \partial_{\xi\xi} y + \partial_{\xi}(y \partial_{\xi} G) + u \partial_{\xi}(y \partial_{\xi} H) + u \partial_{\xi}(x_{\infty} \partial_{\xi} H), \quad \xi \in \Omega, \\ 0 &= [\partial_{\xi} y + y \partial_{\xi} G + u(y + x_{\infty}) \partial_{\xi} H]|_{\xi \in \partial\Omega}. \end{aligned}$$

The control objective consists now in driving y to zero. To compute the controller we further introduce a positive, i.e. destabilising, shift by adding σy to the right hand side of (3.5). If this controller is applied to the unshifted equation it accelerates convergence of y to 0 and hence the convergence of x to x_{∞} .

Considering the variational form of (3.5) one observes that the control will not have an effect on a subspace of co-dimension one. For this reason we introduce $Y_{\mathcal{P}} = \{v \in L^2(\Omega) : \int_{\Omega} v d\xi = 0\}$, and denote by $\mathcal{P} \in \mathcal{L}(L^2(\Omega), Y_{\mathcal{P}})$ the projection onto $Y_{\mathcal{P}}$ along x_{∞} , which is given by $\mathcal{P}y = y - (\int_{\Omega} y d\xi) x_{\infty}$. Subsequently we apply \mathcal{P} to (3.5) with initial datum given by $\mathcal{P}x(0)$. For the details we refer to [42].

The Fokker-Planck equation (3.5) is discretized using a finite difference scheme with D intervals. To allow for possible further reduction of the dimension a balanced

truncation based model reduction, adapted to bilinear systems [41], is used, to reduce the system to dimension d .

For the numerical results we fix $\gamma = 10^{-2}$, $\nu = 1$, $\sigma = 0.2$, and the potentials $G(\xi)$ and $H(\xi)$ are chosen to reproduce the setting in [43], as shown in Fig. 3.8. That is, the ground potential is set to be

$$(3.6) \quad G(\xi) = \frac{((0.5\xi^2 - 15)\xi^2 + 119)\xi^2 + 28\xi + 50}{200},$$

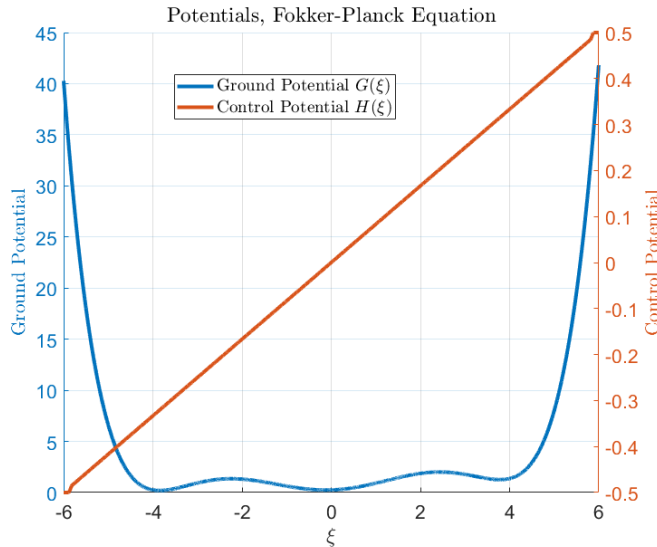
whereas $H(\xi)$ is given by

$$(3.7) \quad H(\xi) = \begin{cases} -1/2 & \text{if } -6.0 \leq \xi \leq -5.9 \\ \xi/12 & \text{if } -5.8 \leq \xi \leq 5.8 \\ 1/2 & \text{if } 5.9 \leq \xi \leq 6.0 \end{cases}$$

with the disjoint intervals united with an Hermite interpolant.

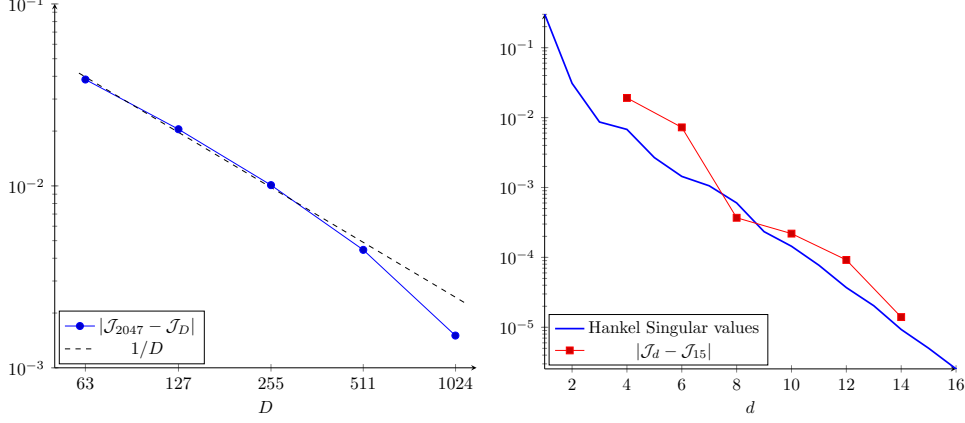
Since both the original system size D , and the reduced dimension d , are approximation parameters, we need to set them to appropriate values that deliver a desired accuracy in the model outcomes, such as the total cost. Note also that in contrast to the linear case, the generalized balanced truncation method for bilinear systems does not exhibit an a priori error bound [41].

Fig. 3.8: Ground and control potentials in the Fokker-Planck control system.



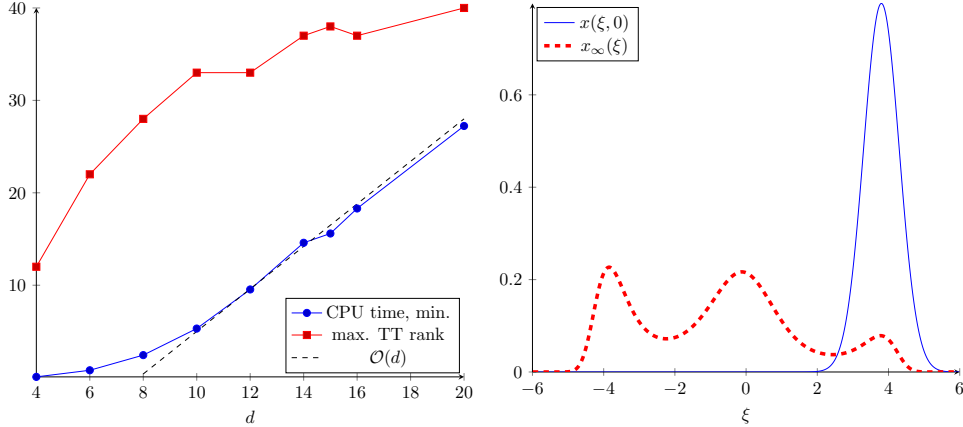
In Fig. 3.9 (left) we study the total cost in the LQR stabilised system. Here we initialise the Fokker-Planck system with the density function of the uniform distribution on $[-6, 6]$. We can deduce that an absolute error of about 10^{-3} (a relative error of 1%) is achieved for 1023 points in the initial finite difference discretization. Setting $D = 1023$ and varying the basis size in the balanced truncation, we compare the Hankel singular values and the differences in the total cost in the HJB stabilised system in Fig. 3.9 (right). We observe that $d = 10$ dimensions in the reduced model are sufficient to drop the absolute error below the same level of 10^{-3} .

Fig. 3.9: Errors in the total cost in the Fokker-Planck model with the uniform initial state $x(\xi, 0) = \frac{1}{12}$ for different numbers of discretisation points (left) and different dimensions of the reduced model (right).



In Fig. 3.10 (left) we vary the dimension d of the reduced state and investigate CPU times and TT ranks of the value function. The TT approximation threshold $\delta = 10^{-4}$, the initial shift in Alg. 2.3 $\mu = 5$, and the polynomial degree $n - 1 = 4$. We see that the TT ranks stabilize as the dimension increases, and hence the CPU time grows linearly.

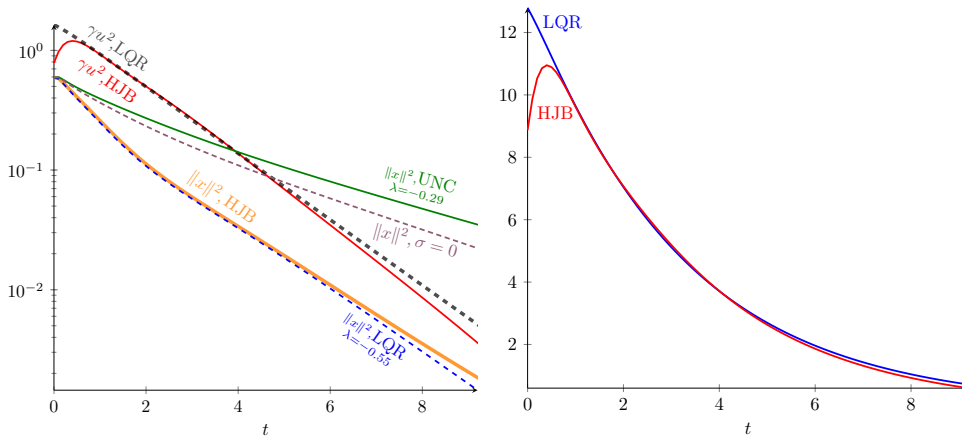
Fig. 3.10: Left: CPU times and TT ranks for different dimensions d for the Fokker-Planck problem with the right-sided initial state $x(\xi, 0) = \frac{1}{Z} \exp(-2(\xi - 3.8)^2)$. Right: initial and equilibrium states.



Moreover, we change the initial distribution to the right-sided state $x(\xi, 0) = \frac{1}{Z} \exp(-2(\xi - 3.8)^2)$, where $Z = \int_{-6}^6 \exp(-2(\xi - 3.8)^2) d\xi$ is the normalisation constant (Fig 3.10, right). It was observed [43] that the free system exhibits a very slow convergence to equilibrium when started from a right-sided distribution, since the particles must flow through a region of low probability. In Fig. 3.11 we show the

components of the running cost for the *original* unshifted system, both UNControlled and controlled with HJB and LQR signals, obtained for the shifted system. We see that the free system converges at a slow rate $\|x\|^2 \sim \exp(-0.29t)$, while the controller computed for the de-stabilised system can accelerate this rate by almost a factor of 2. Note that when the HJB controller is computed for the original system ($\sigma = 0$), it accelerates the convergence only a little, so the shift is important to achieve the speedup. However, larger shifts make the HJB equation more difficult to solve. In particular, for larger shifts σ and larger state domain sizes a the stiffness matrix in (2.12) might become indefinite, and the policy iteration fails to converge. The domain size should be large enough to fit the trajectory, e.g. for the right-sided initial state the domain size of $a = 20$ is necessary to avoid excessive extrapolation of Legendre polynomials. This poses certain limitations on the range of possible applications of the TT-HJB approach. Nevertheless, when the policy iteration converges the HJB regulator can deliver a lower cost than LQR.

Fig. 3.11: Running costs (left) and control signals (right) for the reduced Fokker-Planck problem with $d = 10$ with the right-sided initial state $x(\xi, 0) = \frac{1}{2} \exp(-2(\xi - 3.8)^2)$.



REFERENCES

- [1] G. Albi, Y.-P. Choi, M. Fornasier and D. Kalise. *Mean Field Control Hierarchy*, Appl. Math. Optim. 76(1)(2017):93–135.
- [2] A. Alla, M. Falcone and D. Kalise. *An efficient policy iteration algorithm for dynamic programming equations*, SIAM J. Sci. Comput., 37(1)(2015):A181–A200, 2015.
- [3] A. Alla, M. Falcone and S. Volkwein. *Error Analysis for POD Approximations of Infinite Horizon Problems via the Dynamic Programming Approach*, SIAM J. Control Optim. 55(5)(2017):3091–3115.
- [4] A. Alla, M. Falcone and L. Saluzzi. *An Efficient DP Algorithm on a Tree-Structure for Finite Horizon Optimal Control Problems*, SIAM J. Sci. Comput. 41(4)(2019):A2384–A2406
- [5] M. Akian, S. Gaubert and A. Lakhoua. *The Max-Plus Finite Element Method for Solving Deterministic Optimal Control Problems: Basic Properties and Convergence Analysis*, SIAM J. Control Optim. 47(2)(2008):817–848.
- [6] R. W. Beard, G. N. , and J. T. Wen. *Galerkin approximation of the Generalized Hamilton-Jacobi-Bellman equation*, Automatica 33(12)(1997) 2159–2177.
- [7] G. Belykin and M. Mohlenkamp. *Numerical operator calculus in higher dimensions*, Proc. Natl. Acad. Sci., 99(2002):10246–10251.

- [8] D. P. Bertsekas. *Reinforcement Learning and Optimal Control*, Athena Scientific, Belmont, Massachusetts, 2019.
- [9] J.-M. Biannic and J. Boada-Bauxel. *A Civilian Aircraft Landing Challenge*, <https://w3.onera.fr/smac> (2016).
- [10] O. Bokanowski, J. Garcke, M. Griebel, and I. Klompaker. *An Adaptive Sparse Grid Semi-Lagrangian Scheme for First Order Hamilton-Jacobi Bellman Equations*, *J. Sci. Comput.* 55(3)(2013):575-605.
- [11] O. Bokanowski, S. Maroso and H. Zidani. *Some Properties of Howards' Algorithm*, *SIAM J. Numer. Anal.* 47(4)(2009):3001-3026.
- [12] Y.T. Chow, J. Darbon, S. Osher and W. Yin. *Algorithm for overcoming the curse of dimensionality for state-dependent Hamilton-Jacobi equations*, *J. Comput. Phys.* 387(2019):376-409.
- [13] M.G. Crandall and P.L. Lions. *Two approximations of solutions of Hamilton-Jacobi equations*, *Math. Comp.* 43(167)(1984):1-19.
- [14] M.G. Crandall and P.L. Lions. *Hamilton-Jacobi equations in infinite dimensions I. Uniqueness of viscosity solutions*, *J. Funct. Anal.* 62(3)(1985):379-396.
- [15] W. E, J. Han, and A. Jentzen. *Deep learning-based numerical methods for high-dimensional parabolic partial differential equations and backward stochastic differential equations*, *Comm. Math. Stat.* 5(4)(2017):349-380.
- [16] M. Falcone, and R. Ferretti. *Numerical methods for Hamilton-Jacobi type equations*, *Handb. Numer. Anal.* 17(2016):603-626.
- [17] J. Garcke and A. Kröner. *Suboptimal feedback control of PDEs by solving HJB equations on adaptive sparse grids*, *J. Sci. Comput.*, doi:10.1007/s10915-016-0240-7 (2016).
- [18] M. B. Horowitz, A. Damle and J. W. Burdick. *Linear Hamilton Jacobi Bellman equations in high dimensions*, *Proc. IEEE/CDC* 2014:5880-5887.
- [19] C. Huré, H. Pham and X. Warin. *Some machine learning schemes for high-dimensional nonlinear PDEs*, arXiv:1902.01599 (2019).
- [20] D. Kalise and A. Kröner. *Reduced-order minimum time control of advection-reaction-diffusion systems via dynamic programming*, *Proc. 21st International Symposium on Mathematical Theory of networks and Systems*, 1196-1202 (2014).
- [21] D. Kalise and K. Kunisch. *Polynomial approximation of high-dimensional Hamilton-Jacobi-Bellman equations and applications to feedback control of semilinear parabolic PDEs*, *SIAM J. Sci. Comput.* 40(2)(2018):629-652.
- [22] D. Kalise, S. Kundu, and K. Kunisch. *Robust feedback control of nonlinear PDEs by numerical approximation of high-dimensional Hamilton-Jacobi-Isaacs equations*, arXiv:1905.06276, 2019.
- [23] W. Kang and L. Wilcox. *Mitigating the Curse of Dimensionality: Sparse Grid Characteristics Method for Optimal Feedback Control and HJB Equations*, *Comput. Optim. Appl.* 68(2)(2017):289-315.
- [24] B. Khoromskij. *Tensor numerical methods for multidimensional PDEs: theoretical analysis and applications*, *ESAIM: Proc.* 48(2015):1-28.
- [25] W. Hackbusch. *Tensor Spaces And Numerical Tensor Calculus*, Springer-Verlag, Berlin, 2012.
- [26] T. Kolda and B. Bader. *Tensor Decompositions and Applications*, *SIAM Rev.* 51(3)(2009):455-500.
- [27] K. Kunisch, S. Volkwein, L. Xie. *HJB-POD Based Feedback Design for the Optimal Control of Evolution Problems*, *SIAM J. Appl. Dyn. Sys.* 4(2004):701-722.
- [28] S.E. Lyshevski. *Optimal control of nonlinear continuous-time systems: design of bounded controllers via generalized nonquadratic functionals*, *Proc. American Control Conf.* 1998, pp. 205-209.
- [29] W. M. McEneaney. *A curse-of-dimensionality-free numerical method for solution of certain HJB PDEs*, *SIAM J. Control Optim.* 46(4)(2007):1239-1276.
- [30] T. Nakamura-Zimmerer, Q. Gong and W. Kang. *Adaptive Deep Learning for High Dimensional Hamilton-Jacobi-Bellman Equations*, arXiv:1907.05317, 2019.
- [31] M. Neilan, A.J. Salgado and W. Zhang. *Numerical analysis of strongly nonlinear PDEs*, *Acta Numerica* 26(2017):137-303.
- [32] I. V. Oseledets. *Tensor-Train Decomposition*, *SIAM J. Sci. Comput.*, 33(5)(2011):2295-2317.
- [33] M. Raissi and G.E. Karniadakis. *Hidden physics models: Machine learning of nonlinear partial differential equations*, *J. Comput. Phys.* 357(2018):125-141.
- [34] C. Reisinger and Y. Zhang. *Rectified deep neural networks overcome the curse of dimensionality for nonsmooth value functions in zero-sum games of nonlinear stiff systems*, arXiv:1903.06652, 2019.
- [35] J. G. Verwer and J. M. Sanz-Serna. *Convergence of method of lines approximations to partial differential equations*, *Computing* 33(3-4)(1984):297-313.

- [36] D. Savostyanov, S. Dolgov, J. Werner and I. Kuprov. *Exact NMR simulation of protein-size spin systems using tensor train formalism*, Phys. Rev. B 90(2014):085139.
- [37] J. Sirignano and K. Spiliopoulos. *DGM: A deep learning algorithm for solving partial differential equations*, J. Comput. Phys. 375(2018):1339–1364.
- [38] E. Todorov. *Efficient computation of optimal actions*, Proc. Nat. Acad. Sci. 106(28)(2009):11478–11483.
- [39] I. Yegorov and P.M. Dower. *Perspectives on Characteristics Based Curse-of-Dimensionality-Free Numerical Approaches for Solving HamiltonJacobi Equations*, Appl Math Optim (2018).
- [40] J. Ballani and L. Grasedyck, *A projection method to solve linear systems in tensor format*, Numerical Linear Algebra with Applications, 20 (2013):27–43.
- [41] P. Benner and T. Damm, *Lyapunov equations, energy functionals, and model order reduction of bilinear and stochastic systems*, SIAM Journal on Control and Optimization, 49 (2011):686–711.
- [42] T. Breiten, K. Kunisch, and L. Pfeiffer, *Infinite-horizon bilinear optimal control problems: Sensitivity analysis and polynomial feedback laws*, SIAM Journal on Control and Optimization, 56 (2018):3184–3214.
- [43] T. Breiten, K. Kunisch, and L. Pfeiffer, *Numerical study of polynomial feedback laws for a bilinear control problem*, Mathematical Control and Related Fields, 8 (2018):557.
- [44] S. Dolgov and B. Khoromskij, *Two-level QTT-Tucker format for optimized tensor calculus*, SIAM J. on Matrix An. Appl., 34 (2013):593–623.
- [45] S. V. Dolgov and D. V. Savostyanov, *Alternating minimal energy methods for linear systems in higher dimensions*, SIAM J. Sci. Comput., 36 (2014):A2248–A2271.
- [46] Y. Eidelman and I. Gohberg, *On a new class of structured matrices*, Integral Equations and Operator Theory, 34 (1999):293–324.
- [47] S. A. Goreinov, I. V. Oseledets, D. V. Savostyanov, E. E. Tyrtyshnikov, and N. L. Zamarashkin, *How to find a good submatrix*, in Matrix Methods: Theory, Algorithms, Applications, V. Olshevsky and E. Tyrtyshnikov, eds., World Scientific, Hackensack, NY (2010):247–256.
- [48] L. Grasedyck, *Existence and computation of low Kronecker-rank approximations for large systems in tensor product structure*, Computing, 72 (2004):247–265.
- [49] W. Hackbusch, *A sparse matrix arithmetic based on \mathcal{H} -matrices. Part I: Introduction to \mathcal{H} -matrices*, Computing, 62 (1999):89–108.
- [50] C. Hartmann, B. Schäfer-Bund, and A. Thöns-Zueva, *Balanced averaging of bilinear systems with applications to stochastic control*, SIAM Journal on Control and Optimization, 51 (2013):2356–2378.
- [51] S. Holtz, T. Rohwedder, and R. Schneider, *The alternating linear scheme for tensor optimization in the tensor train format*, SIAM J. Sci. Comput., 34 (2012):A683–A713.
- [52] B. Khoromskij and C. Schwab, *Tensor-structured Galerkin approximation of parametric and stochastic elliptic PDEs*, SIAM J. Sci. Comput., 33 (2011):1–25.
- [53] D. Kressner and C. Tobler, *Low-rank tensor Krylov subspace methods for parametrized linear systems*, SIAM J. Matrix Anal. Appl., 32 (2011):273–290.
- [54] B. J. Matkowsky and Z. Schuss, *Eigenvalues of the Fokker-Planck operator and the approach to equilibrium for diffusions in potential fields*, SIAM Journal on Applied Mathematics, 40 (1981):242–254.
- [55] I. V. Oseledets, *Constructive representation of functions in low-rank tensor formats*, Constr. Approx., 37 (2013):1–18.
- [56] I. V. Oseledets and S. V. Dolgov, *Solution of linear systems and matrix inversion in the TT-format*, SIAM J. Sci. Comput., 34 (2012):A2718–A2739.
- [57] I. V. Oseledets and E. E. Tyrtyshnikov, *TT-cross approximation for multidimensional arrays*, Linear Algebra Appl., 432 (2010):70–88.
- [58] D. V. Savostyanov, *Quasioptimality of maximum-volume cross interpolation of tensors*, Linear Algebra Appl., 458 (2014):217–244.
- [59] R. Schneider and A. Uschmajew, *Approximation rates for the hierarchical tensor format in periodic Sobolev spaces*, Journal of Complexity, (2013).
- [60] T. Breiten, K. Kunisch and L. Pfeiffer, *Feedback stabilization of the two-dimensional Navier-Stokes equations by value function approximation*, arXiv:1902.00394, 2019.
- [61] L. N. Trefethen, *Spectral methods in MATLAB*, SIAM, Philadelphia, 2000.
- [62] E. E. Tyrtyshnikov, *Tensor approximations of matrices generated by asymptotically smooth functions*, Sbornik: Mathematics, 194 (2003):941–954.